

Department of Physics and Astronomy
University of Heidelberg

Bachelor Thesis in Physics
submitted by

Lucas Altenkämper

born in Freiburg (Germany)

2014

ALICE Capabilities for Reconstructing neutral Pions by Pairing Photons from the Conversion Method and Calorimeters

This Bachelor Thesis has been carried out by Lucas Altenkämper at the
Physikalisches Institut at the University of Heidelberg
under the supervision of
PD Dr. Klaus Reygers

ALICE Capabilities for Reconstructing neutral Pions by Pairing Photons from the Conversion Method and Calorimeters

In this thesis, a study of ALICE capabilities to reconstruct neutral pions from the two photon decay channel and calculate the direct photon fraction by the combination of photons from the conversion method with photons from calorimeter measurements is presented. Therefore a simple simulation of π^0 decays is done and photons measured via conversion are tagged as coming from such a decay, if the second photon is found in a calorimeter. The systematic uncertainties of the pion decay tagged photon acceptance are studied and compared with the default methods used for neutral pion reconstruction. Additionally, peak positions and widths from π^0 analysis using different methods are compared.

Fähigkeit des ALICE Detektors zur Rekonstruktion neutraler Pionen durch Paarung von Photonen gemessen durch Konversion und in den Kalorimetern

In dieser Arbeit wird eine Machbarkeitsstudie zur Rekonstruktion neutraler Pionen aus dem Zerfallskanal in zwei Photonen, sowie der Berechnung des Anteils direkter Photonen am kompletten Photonsignal der Kollision aus der Kombination von Photonen, die über Konversion gemessen wurden, mit Photonen aus den Kalorimetern, präsentiert. Für diese Studie wurden π^0 Zerfälle simuliert und zu Photonen, die über Konversion gemessen wurden, Partner in den Kalorimetern gesucht. Die systematischen Unsicherheiten der so bestimmten Akzeptanz werden untersucht und mit den Standardmethoden zur Rekonstruktion neutraler Pionen verglichen. Zusätzlich wird eine π^0 Analyse mit den verschiedenen Methoden durchgeführt und die Position sowie Breite der Peaks betrachtet.

Acknowledgements

First of all, I would like to thank my supervisor PD Dr. Klaus Reygers for the opportunity to study the interesting topic of photon physics within the frame of high energy particle physics and carry out my bachelor thesis in the ALICE group. The guidance and the support I got were very helpful for the realisation of this thesis. Secondly I would like to thank Dr. Kai Schweda for the reading and second evaluation of this thesis.

I would like to express special thanks to Friederike Bock and Lucia Leardini for their help and patience. If it wasn't for them, I would not have learned so much about the analysis process. I am also in great debt to Friederike Bock and Baldo Sahlmüller for the implementation of the method presented in this thesis in the analysis framework. Otherwise I would not be able to present the two neutral pion analysis plots.

Also I would like to thank the ALICE group at Heidelberg and CERN for the welcoming environment, the support and fruitful discussions that helped me throughout the process of producing this work.

Finally, I would like to express my acknowledgements for my family, my girlfriend Sarah and my friends for their patience and support. I appreciate this a lot.

Preface

In order to simplify the notation, natural units are used in this work. This especially applies for $c = 1$, so that momenta, masses as well as energies are expressed in units of energy.

Contents

1. Introduction	3
2. Theoretical Background	5
2.1. Quantum Chromodynamics	5
2.2. The Quark Gluon Plasma	6
3. Photons in heavy ion collisions	9
3.1. Direct Photons	9
3.2. Direct photon fraction	11
3.3. π^0 tagging method	13
4. The Experimental Setup	17
4.1. Inner Tracking System	18
4.2. Time Projection Chamber	18
4.3. Electromagnetic Calorimeter	19
4.4. Photon Spectrometer	19
5. π^0 tagged photon acceptance in ALICE	21
5.1. Monte Carlo simulation	21
5.2. Detector description	23
5.3. Tagging acceptance	25
5.4. Systematics of tagging method	26

5.5. Validation of simulation procedure	31
6. Conclusion	37
7. Outlook	39
8. Bibliography	43
A. Appendix	45
A.1. Systematic uncertainties on photon double ratio	45
A.2. Systematic uncertainties on pion tagged photon acceptance	47

1. Introduction

It is assumed, that shortly after the Big Bang, the universe was in a very hot and dense state, called the Quark Gluon Plasma (QGP) which then froze out and hadronized. Where in the universe as it is today the QGP may only exist in the center of neutron stars, it can be created from the collision of heavy nuclei with highly relativistic energies in collider experiments. The research for the QGP started in the end of the 1980's with the Super Proton Synchrotron (SPS) at CERN being the first collider that may have already produced an intermediate state between the plasma and the hadron gas. With the Relativistic Heavy Ion Collider (RHIC) at the Brookhaven National Laboratory higher energies were reached and indications for the creation of the QGP were observed in the collision of gold nuclei. The Large Hadron Collider (LHC) at CERN now offers the highest center of mass energies ever reached and should therefore provide the needed energies and particle densities to create the plasma which is studied by the ALICE experiment.

Although it is experimentally difficult to distinguish between the different sources of photons emerging from the QGP, they are a great probe since the strongly interacting medium will be mostly transparent for them. A main task when studying photons is the determination of the spectrum of decay photons that emerge from the electromagnetic decays of particles produced in the collision. This is generally done by determining the yield of photons that emerge from the decay of neutral pions and then calculating the total decay spectrum with the use of computer based simulations.

In this thesis, a method for the determination of the π^0 decay photon spectrum is

presented and tested for ALICE capabilities, that already is in use at the PHENIX experiment at RHIC. Until now photons from the decay channel $\pi^0 \rightarrow \gamma\gamma$ are measured solely via conversion or in the calorimeters, whereas this new method will pair photons that were reconstructed from a converted e^+e^- pair with photons from a calorimeter.

At first the theoretical background consisting of QCD and the QGP will be introduced with a focus on photons in heavy ion collisions in the following. Also the default methods for neutral pion decay photons analysis will be presented in the frame of the direct photon fraction. Then the detectors from ALICE that are needed for this study will be addressed. Last, the study of the new method will be covered with a focus on the comparison of the systematic uncertainties with the default methods.

2. Theoretical Background

2.1. Quantum Chromodynamics

Quantum Chromodynamics (QCD) is a theory that describes the interaction between particles carrying color-charge, namely quarks and gluons, driven by the strong force. In analogy to electromagnetism the quantum number color behaves like a charge with the gluon as mediating particle. In contrast to the electromagnetic interaction, also gluon-gluon vertices are possible since the gluon carries color-charge.

The potential between quarks and antiquarks can be approximated by:

$$V(r) = -\frac{4}{3} \frac{\alpha_s}{r} + kr \tag{2.1.1}$$

In comparison to the electroweak theory, combining the electromagnetic and weak interaction, the coupling constant in QCD is much higher ($\alpha_s \approx 1 \gg \alpha_{em} \approx \frac{1}{137}$). Since α_s changes as a function of energy and momentum transfer it is called a running constant. For small r the first term dominates and the potential behaves like a Coulomb interaction. In the limit $r \rightarrow 0$ the momentum transfer increases dramatically and α_s approaches zero. This is called asymptotic freedom and perturbative calculations can be used. Going to large distances, or low momentum transfers respectively, the linear part starts to dominate and the coupling constant increases to $O(1)$. To separate a quark-antiquark pair infinite energy would be needed, therefore at some point it is

energetically favorable to create a new pair from the vacuum. Because of this behavior, called confinement, free quarks can't be observed in nature. Instead quarks are always bound in color-neutral states, that are baryons and their anti-particles, consisting of three quarks or antiquarks respectively or mesons, which are quark-antiquark pairs.

2.2. The Quark Gluon Plasma

The binding of quarks and gluons to hadronic states starts to dissolve, when going to higher temperatures and densities. This phase transition to a deconfined state, called the Quark Gluon Plasma (QGP), occurs at a critical temperature T_c , shown in figure 2.2.1, that can be calculated using Lattice QCD (LQCD). Quarks and gluons can move freely in the plasma due to the asymptotic freedom of the quark-antiquark potential and only start to stick together again when the system freezes out. It is thought that the universe was in the state of the Quark Gluon Plasma shortly after the Big Bang [1]. From the collision of heavy nuclei at highly relativistic energies, the QGP can also be established in a laboratory. The first accelerator that might have produced an intermediate state between the hadron gas and the quark gluon plasma was the Super Proton Synchrotron (SPS) at CERN in the late 1980's, operating at center of mass energies of $\sqrt{s_{NN}} = 17.2$ GeV per nucleon pair. Indications for an established quark gluon plasma were then observed at the Relativistic Heavy Ion Collider (RHIC) at the Brookhaven National Laboratory (BNL) that reached energies of $\sqrt{s_{NN}} = 200$ GeV per nucleon pair. The Large Hadron Collider (LHC) at CERN reaches energies more than a factor of 10 larger than at RHIC, that should produce the needed conditions for the quark gluon plasma to emerge.

Even if the existence of the QGP only lasts some microseconds, the system should approach local equilibrium and thermodynamic quantities like temperature, pressure and density can be defined. Furthermore the QGP behaves like a near-ideal liquid and shows characteristics like flow in general and more specific anisotropic flow if the

overlap region of the colliding nuclei is not symmetric. This anisotropy highly depends on the hydrodynamical evolution of the system and is therefore a strong indicator for the presence of the quark gluon plasma.

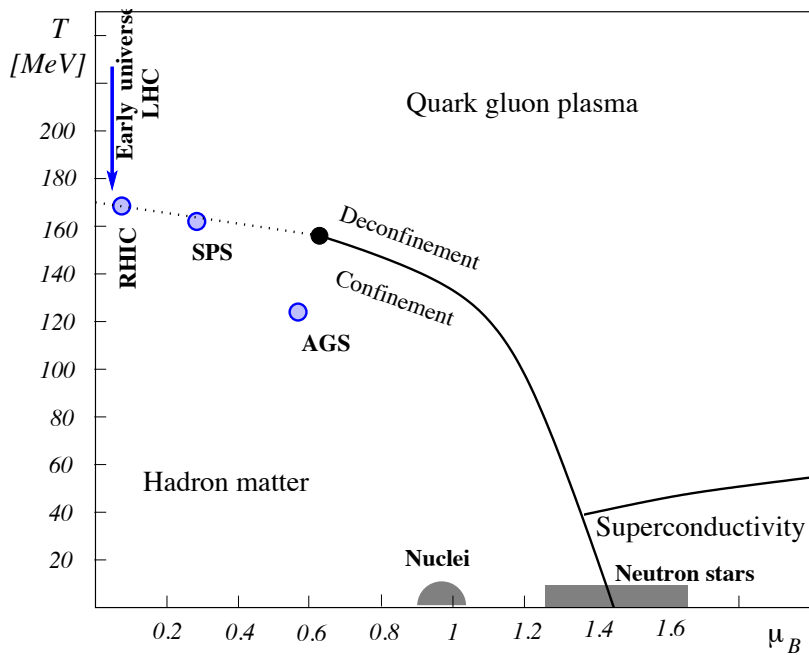


Figure 2.2.1.: Schematic QCD phase diagram that shows confinement to hadronic matter at low T and μ_B . Deconfinement occurs at some critical temperature $T_c \approx 170$ MeV. [9]

3. Photons in heavy ion collisions

In heavy ion collisions, photons are produced in several ways, that can be separated in two main groups: Direct photons that are produced in some sort of particle collision or interaction and decay photons that are emitted from electromagnetically decaying particles, such as $\pi^0 \rightarrow \gamma\gamma$.

Photons are a very interesting observable when looking at the quark gluon plasma since they only interact electromagnetically. Due to the much smaller coupling constant for electromagnetic processes in comparison to strong interactions, the very dense and strongly interacting QGP will be mostly transparent for photons. Thus we can learn about the conditions under which the photons were produced. On the other hand shows the QGP specific photon signals like an excess in photons from thermal sources, compared to heavy ion collisions where no such medium is created. Photons can therefore be a good indicator for the presence of the medium.

3.1. Direct Photons

Direct photons can emerge from hard scattering of partons like the quark-gluon Compton scattering or quark-antiquark annihilations. The Feynman graphs to these processes are shown in figure 3.1.1. After an initial hard scattering, a photon can be radiated by a quark as a part of the jet fragmentation process, as shown in the left panel in figure 3.1.2. These processes can take place in vacuum and the rates can in principle be calculated in pQCD. The emerging photons are often called prompt photons [10].

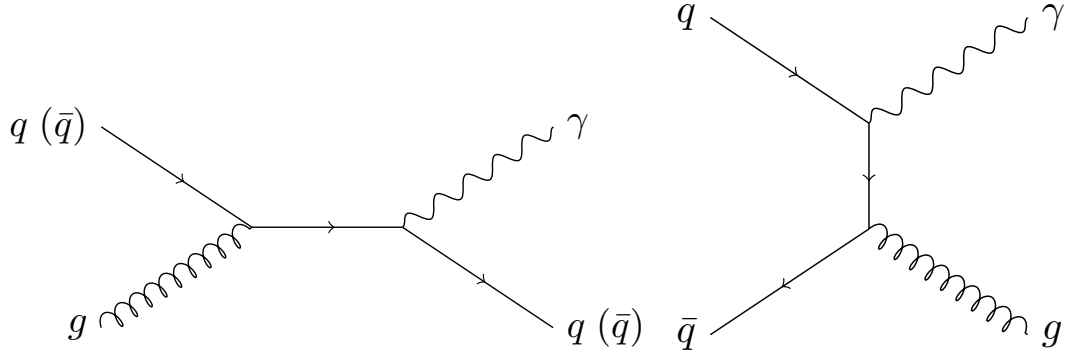


Figure 3.1.1.: left: Quark-gluon Compton scattering $q(\bar{q}) + g \rightarrow q(\bar{q}) + \gamma$, right: Quark-antiquark annihilation $q + \bar{q} \rightarrow g + \gamma$

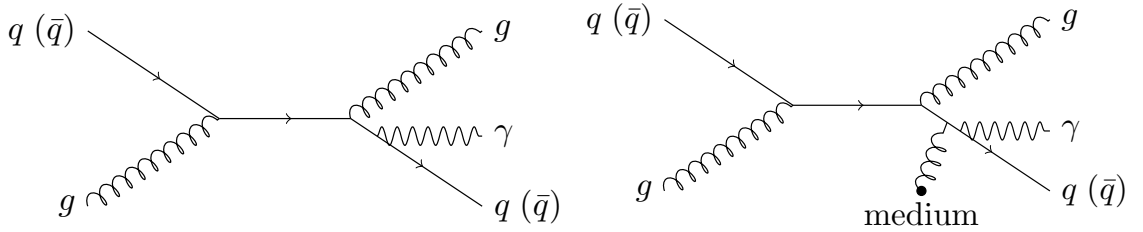


Figure 3.1.2.: left: Quark emits photon as part of jet-fragmentation, $q(\bar{q}) + g \rightarrow q(\bar{q}) + g + \gamma$, right: Quark emits bremsstrahlung-photon through interaction with medium

If a strong interacting medium like the quark gluon plasma is present, photons can also be emitted by parton-medium interactions like quark bremsstrahlung [10]. The corresponding Feynman graph is shown in the right panel in figure 3.1.2. Photons coming from bremsstrahlung as well as from the fragmentation of a quark can be called fragmentation photons.

Besides the already mentioned processes that produce hard photons, also photons following a thermal distribution can be produced in the medium. A hadron gas will already emit thermal photons, but an excess will be observed if the QGP is present due to the local equilibrium the system should be in. Although the term thermal radiation is often used, the QGP is not a black body radiator. These photons are produced with low momentum from the scattering of partons in the thermalized heat bath [10].

Experimentally it is difficult to measure direct photons due to the large background

of decay photons. To distinguish direct photons from decay photons, the source of each photon would have to be known. The invariant yield of direct photons γ_{dir} can be expressed in terms of the invariant yields of all photons emitted without respect to the source, called inclusive photons, γ_{inc} and that of photons coming from particle decays γ_{dec} :

$$\gamma_{dir}(p_T) = \gamma_{inc}(p_T) - \gamma_{dec}(p_T). \quad (3.1.1)$$

3.2. Direct photon fraction

A measurement of the presence of direct photons is the fraction of inclusive photons above decay photons, here addressed as the direct photon fraction R_γ . The direct photon invariant yield can be rewritten in terms of the inclusive photons, using R_γ :

$$\gamma_{dir}(p_T) = \gamma_{inc}(p_T) \cdot \left(1 - \frac{\gamma_{dec}(p_T)}{\gamma_{inc}(p_T)}\right) = \gamma_{inc}(p_T) \cdot \left(1 - R_\gamma^{-1}(p_T)\right) \quad (3.2.1)$$

This is favorable since only the direct photon fraction has to be calculated to observe direct photons in the inclusive sample. If it exceeds unity, direct photons are produced in the collision. The fraction can in general be calculated with the use of computer based simulations of the decay photon spectrum. Hence the invariant decay photon yield doesn't have to be reconstructed from data. Since the primary source of decay photons is the decay of neutral pions to two photons with a branching ratio above 98%, which typically makes up 85 – 90% of all decay photons [10], it is useful to reconstruct the invariant π^0 yield to normalize measured data to simulation. Also the systematic uncertainties that affect the photon and neutral pion yields in the same way will cancel in the ratio. With the invariant π^0 yield from simulation, R_γ takes the form :

$$R_\gamma(p_T) = \frac{\gamma_{inc}(p_T)}{\gamma_{dec}(p_T)} = \frac{\left(\frac{\gamma_{inc}(p_T)}{\pi^0(p_T)}\right)_{data}}{\left(\frac{\gamma_{dec}(p_T)}{\pi^0(p_T)}\right)_{sim}} \quad (3.2.2)$$

The direct photon fraction following this definition is often called the photon double ratio and is experimentally useful due to the cancellation of systematics. Although the uncertainties will not cancel completely, they will at least partially drop out. The uncertainties that are carried by the invariant yields depend on the methods that are used to measure the photons or neutral pions respectively. There are two default methods to reconstruct neutral pions from the two photon decay channel used in ALICE: The Photon Conversion Method (PCM) that reconstructs photons from pair creation in the central tracking system and measuring both photons in a calorimeter, which was already done for PHOS [4].

Photon conversion method Photons will convert to electron-positron pairs in the detector material of the Inner Tracking System (ITS) and the Time Projection Chamber (TPC) with a probability of $(8.6 \pm 0.4)\%$ [4]. By measuring the tracks of a created e^+e^- pair in an outer magnetic field, the momentum of the mother photon can be reconstructed. This gives a very good resolution to low transverse momenta but is constrained due to curling of the electron tracks inside the field which can occur below $p_T = 50$ MeV for a single electron or positron. If going to higher p_T the tracks in the magnetic field will get less bent and the resolution in the reconstruction will decrease. When building the double ratio from photons and neutral pions measured with the conversion method, the conversion probability, that is a strongly material dependent quantity, plays a crucial role in the systematic uncertainty since it remains once in R_γ . An analysis of the photon double ratio with PCM was done for Pb-Pb collisions at $\sqrt{s_{NN}} = 2.76$ TeV in [11]. The systematic errors for the different centrality classes are shown in figure A.1.1 in the appendix. For each centrality class the total systematic

uncertainty ranges in between 5 – 10% with the material budget being a major source up to $p_T = 5$ GeV. For a more detailed description of the photon conversion method, see [4, 6].

Photons from calorimeter clusters Instead of reconstructing photons from conversion e^+e^- pairs, photons can also be measured in the calorimeter. Calorimeter clusters that pass the photon identification cuts are recognized as a photon signal. Due to the increase in resolution with increasing energy, calorimeter measurements are expected to give better results for higher transverse momenta. Although in high multiplicity environments the resolution will decrease due to shower merging, that becomes more crucial at higher energies. A direct photon analysis, using the photon double ratio calculated from photons measured in PHOS is presented in [12]. The systematic uncertainties that were estimated for this analysis are listed in table A.1.1 in the appendix. The total systematic uncertainty ranges between 7.1 – 8.9% with the dominant sources being the π^0 raw yield extraction as well as the differences in the yields per module.

3.3. π^0 tagging method

Instead of measuring both photons in a calorimeter or reconstructing them from created electron-positron pairs, the π^0 tagging method only takes one photon from conversion. The converted photon is paired with a photon reconstructed in the calorimeter to combine the advantages of both methods presented. This promises a better resolution in an intermediate p_T region compared to conversion or calorimeter only measurements.

The π^0 tagging method, described in [7], is in use at the PHENIX experiment at RHIC to measure low momentum direct photons in the high multiplicity environment of Au-Au collisions at $\sqrt{s_{NN}} = 200$ GeV. It has the definite advantage, that the major sources of systematics, which are at PHENIX the electron pair efficiency and acceptance and the conversion probability, cancel when calculating R_γ . At PHENIX the conversion

probability plays such a crucial role since the material budget, that gives a measure of the conversion probability, is only known within an uncertainty of 30 – 50% [7].

All converted photons measured give the number of inclusive photons that are observed, with γ_{inc} being the true number of photons produced by nature:

$$N_{\gamma}^{inc}(p_T) = c \cdot \epsilon_{e^+e^-}(p_T) a_{e^+e^-}(p_T) \cdot \gamma_{inc}(p_T) \quad (3.3.1)$$

The number of photons depends on the probability that a photon will convert in the material c as well as the acceptance and efficiency for the e^+e^- pair reconstruction $a_{e^+e^-}$ and $\epsilon_{e^+e^-}$ respectively.

For every converted photon measured, an unconverted partner is searched for in a calorimeter. Then the pair invariant mass is calculated and if it corresponds to the neutral pion mass, the converted photon is tagged as coming from a π^0 decay. The number of π^0 decay tagged photons, with the true number of photons produced from neutral pion decays γ_{π^0} , is then given by:

$$N_{\gamma}^{\pi^0 tag}(p_T) = c \cdot \epsilon_{e^+e^-}(p_T) a_{e^+e^-}(p_T) \cdot \langle \epsilon_{\gamma}(p_T) f(p_T) \rangle \cdot \gamma_{\pi^0}(p_T) \quad (3.3.2)$$

Additional factors are f and ϵ_{γ} , namely the pion tagging acceptance and efficiency. The acceptance is the probability of getting the unconverted photon from a π^0 decay into the acceptance of a calorimeter, given the partner photon has been reconstructed via conversion. The brackets around these factors imply an averaging over the transverse momentum of the unconverted photon. All p_T dependent factors of N_{γ}^{inc} and $N_{\gamma}^{\pi^0 tag}$ are functions of the transverse momentum of the converted photon.

When building the photon double ratio from equation (3.3.1) and (3.3.2), the conversion dependent factors cancel out:

$$R_\gamma(p_T) = \frac{\langle \epsilon_\gamma(p_T) f(p_T) \rangle \cdot \left(\frac{N_\gamma^{inc}(p_T)}{N_\gamma^{\pi^0 tag}(p_T)} \right)_{data}}{\left(\frac{N_\gamma^{dec}(p_T)}{N_\gamma^{\pi^0}(p_T)} \right)_{sim}} \quad (3.3.3)$$

The only remaining correction is the efficiency and acceptance of the unconverted photon. This may bring a benefit in the systematic uncertainties if the material budget is not well known. From a simulation the denominator of R_γ is calculated, where N_γ^{dec} is the number of decay photons and $N_\gamma^{\pi^0}$ is the fraction of decay photons that are coming from the decay of neutral pions.

The pion tagging correction, namely the product of the unconverted photon efficiency and acceptance $\langle \epsilon_\gamma f \rangle$, has already been studied for PHENIX in [7]. It has been calculated from the ratio of all pion decay tagged converted photons to all converted photons reconstructed and is shown in figure 3.3.1.

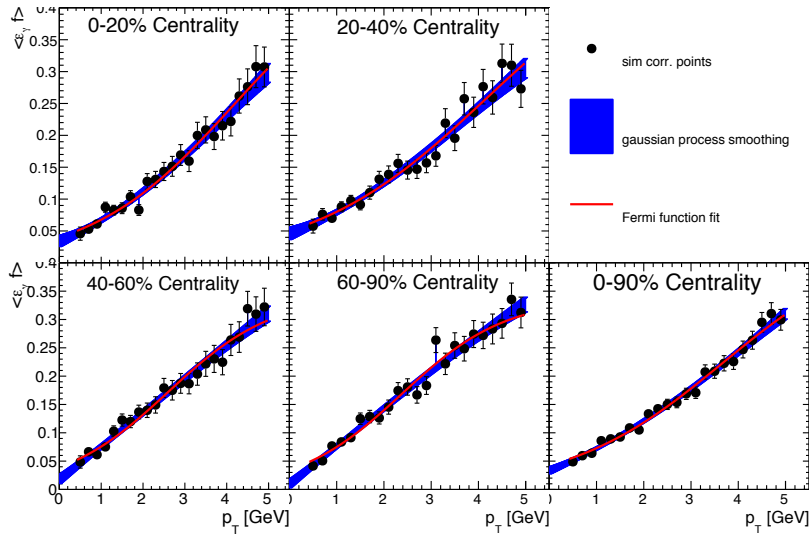


Figure 3.3.1.: Pion tagging correction with a Fermi function fitted to the data points for different centralities. Also a Gaussian Process regression analysis is used to parameterize and smooth the correction. [7]

The relative systematic uncertainties for the photon double ratio that are reached in PHENIX for minimum bias collisions by the use of this method are shown in a low to

intermediate p_T region in figure 3.3.2. The dominant source above $p_T \approx 0.75$ GeV is the uncertainty of the calorimeter energy scale. All systematics are added in quadrature to get the total uncertainty.

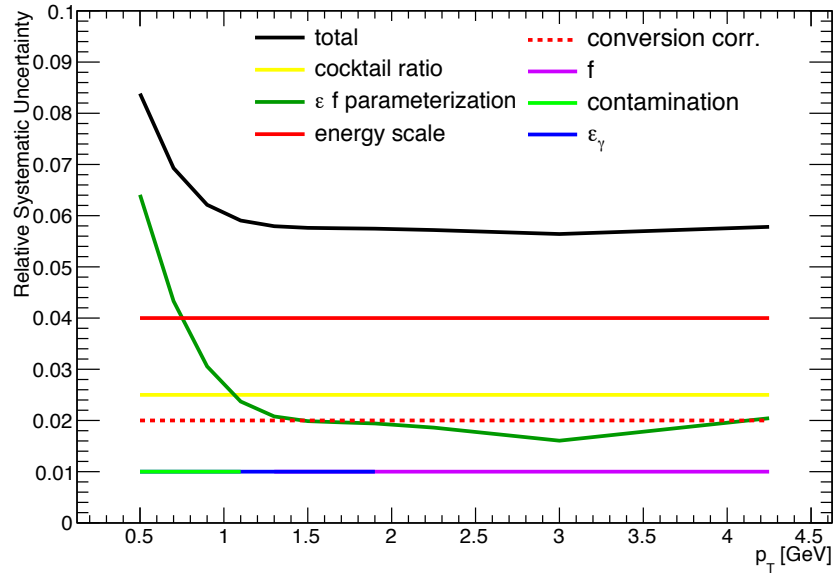


Figure 3.3.2.: Systematic uncertainties on the photon double ratio for minimum bias collisions in PHENIX, using the π^0 tagging method. [7]

4. The Experimental Setup

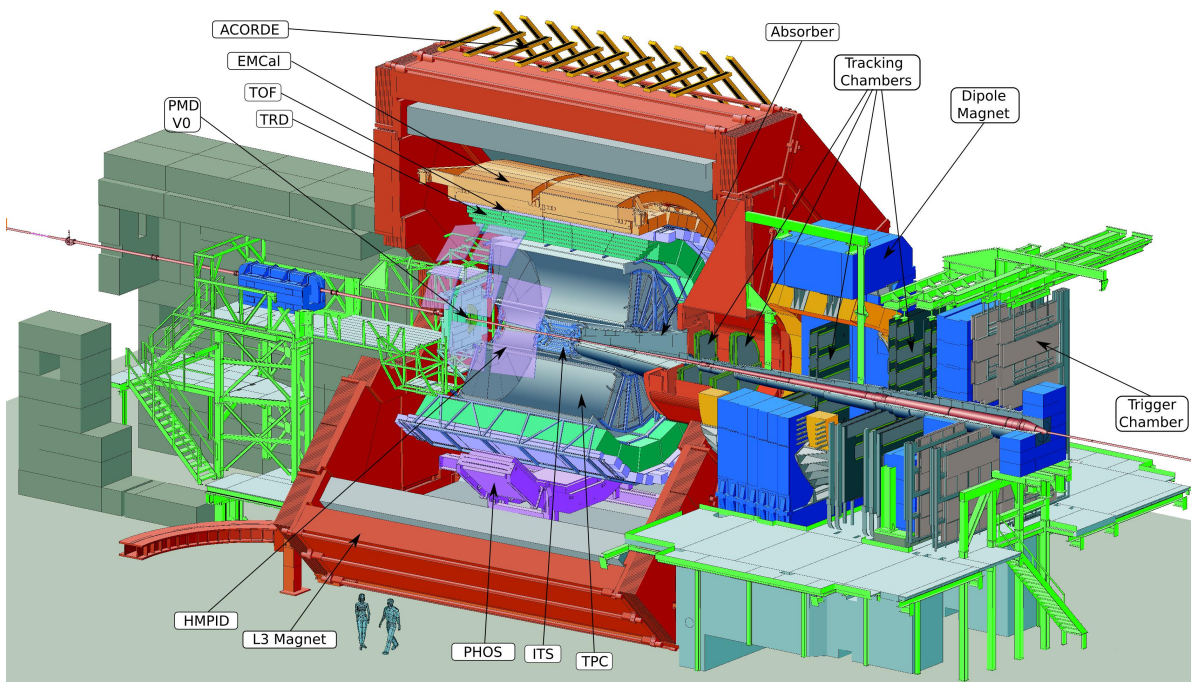


Figure 4.0.1.: The ALICE experiment with it's sub-detectors. [14]

The ALICE detector, shown in figure 4.0.1, is designed to study heavy ion collisions and strongly interacting matter like the quark gluon plasma. Since the study that is presented in this thesis prominently consists of a simple simulation of the acceptances of some of the detectors, the following sections will only describe some parts of the ALICE experiment, crucial for the studied method. The detectors that are represented in the simulation are the Time Projection Chamber to detect converted photons as well as the ElectroMagnetic Calorimeter (EMCal) and the PHOTon Spectrometer (PHOS) for the

calorimeter measurements. The Inner Tracking System (ITS) is also described briefly for completion since it can be used to improve the TPC track measurements, although it is not represented in the simulation. For more detailed information about the ALICE experiment, see [2, 8].

4.1. Inner Tracking System

The Inner Tracking System is a track detector that is able to track and identify particles with momenta below 200 MeV. This can be used to improve the momentum and angular resolution of particles that have been measured in the TPC. The ITS provides 3 different technologies of silicon detectors: Silicon Pixel Detector (SPD), Silicon Drift Detector (SDD) and Silicon Stripe Detector (SSD), each arranged in two layers. All layers cover 2π in azimuth, but different ranges in pseudo-rapidity. The SPD, situated at a radial distance between 3.9 cm and 7.6 cm, covers a pseudo-rapidity range of $|\eta| < 2$ and $|\eta| < 1.4$ referring to the first and second layer. The SDD is located at a radial distance between 15.0 cm and 23.9 cm and covers $|\eta| < 0.9$ in pseudo-rapidity for both layers. The SSD is situated between 38.0 cm and 43.0 cm in radial distance, with both layers covering $|\eta| < 1.0$ in pseudo-rapidity. [4, 6]

4.2. Time Projection Chamber

The TPC is a gas-filled ionization chamber that provides tracking information for charged particles in a high-multiplicity environment up to 8000 particles per rapidity unit. Momentum measurements with a good resolution are possible in a wide range of about $0.1 \text{ GeV} \leq p_T \leq 100 \text{ GeV}$. In addition charged particles can be identified from their specific energy loss per distance dE/dx . The TPC is situated after the ITS at a radial distance of $84.4 \text{ cm} \leq r \leq 246.6 \text{ cm}$ and covers a pseudo-rapidity range of $|\eta| < 0.9$. In azimuth, the full range of 2π is enclosed.

4.3. Electromagnetic Calorimeter

The EMCal is a lead-scintillator sampling calorimeter, located approximately 450 cm in radial distance from the beam pipe. It covers a pseudo-rapidity of $|\eta| < 0.7$ and is situated in the range $80^\circ \leq \phi \leq 187^\circ$ in azimuth [3]. It is designed to study the physics of jet quenching with a focus on high p_T particles. Therefore it has a worse intrinsic energy resolution at lower energies than PHOS, as it can be seen in figure 4.4.1. The energy resolution is given by the quadratic sum of a stochastic term, a noise term and a constant term with the parameters a , b and c respectively:

$$\frac{\sigma}{E} = \frac{a}{\sqrt{E}} \oplus \frac{b}{E} \oplus c \quad (4.3.1)$$

The parameters for the energy resolution are obtained from an electron test beam measurement, shown in figure 4.3.1. They are given by $a = 9.07\%$, $b = 4.35\%$ and $c = 1.63\%$

4.4. Photon Spectrometer

The Photon Spectrometer consists of lead-tungston scintillators with a granularity slightly larger than the Molière radius. It is installed at a radial distance of 460 cm from the interaction point and covers a pseudo-rapidity range of $|\eta| < 0.12$ as well as $260^\circ \leq \phi \leq 320^\circ$ in azimuth [4]. The energy and position resolution of PHOS is very good since it is designed for the measurement of low p_T direct photons. As for EMCal, the energy resolution can be described with equation (4.3.1) with the parameters $a = 3.3\%$, $b = 1.8\%$ and $c = 1.1\%$ obtained from test beam measurements [5]. In figure 4.4.1 the relative energy resolutions for PHOS and EMCal are compared.

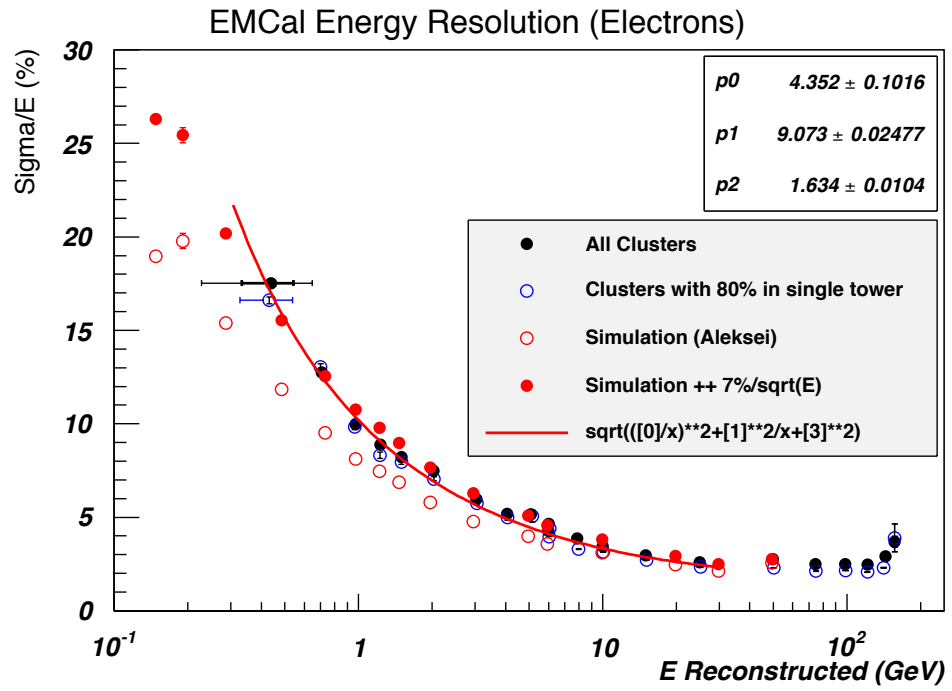


Figure 4.3.1.: EMCAL relative energy resolution from electron test beam.

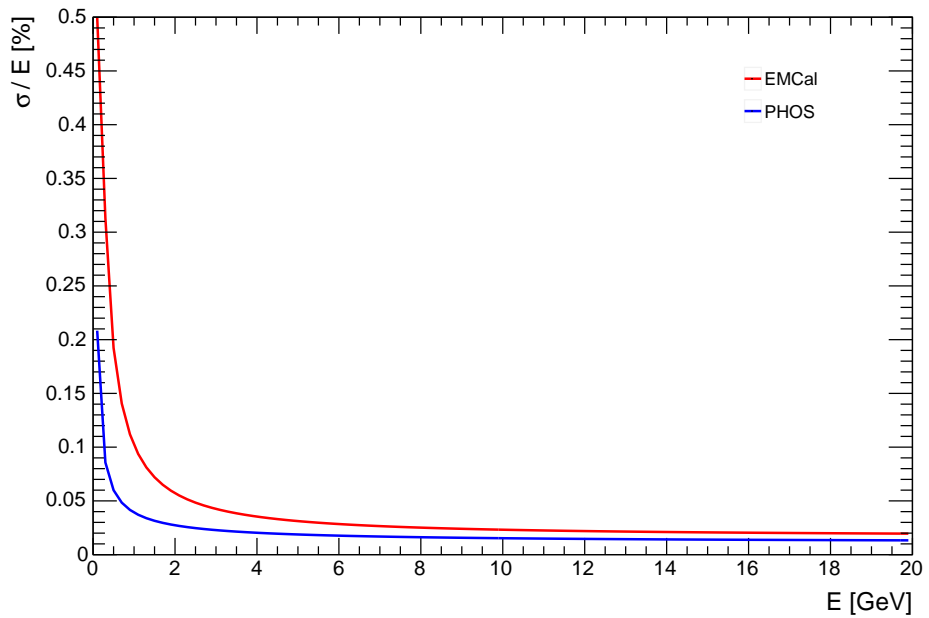


Figure 4.4.1.: Relative energy resolutions described by equation (4.3.1) for PHOS and EMCAL, showing the greater difference to lower energies.

5. π^0 tagged photon acceptance in ALICE

The main focus of this thesis lies on the calculation of the pion tagged photon acceptance with the ALICE detector from a simple simulation of π^0 decays, to estimate if the use of this method brings any advantage, compared to the photon conversion method or to measuring the photons only in the calorimeters. Therefore, also the systematic uncertainties have to be studied in depth. Neutral pions are decayed and the tagging acceptance is calculated as presented from the measured photon spectra in the detectors. In the following sections, the particle decay simulation as well as the representation of the detectors in the course of this simulation will be described. Then the acceptance will be calculated and analysed with a comparison to the default methods for the calculation of the photon double ratio given in section 6. The procedure of this simulation is validated by a comparison with the results from [7] for the PHENIX detector at RHIC energies in section 5.5.

5.1. Monte Carlo simulation

The simulation used is a simplified model that decays neutral pions from which the channel $\pi^0 \rightarrow \gamma\gamma$ will be analysed. Neutral pions are produced and decayed using the PYTHIA 8 particle decayer. To produce more statistics, especially to higher transverse momenta, the pions are first produced flat in p_T with a weight later on applied to describe

their distribution given at LHC energies. The energies and centrality classes that will be looked at are listed in table 5.1.1, where N_{events} refers to the number of produced π^0 . Although no full events are simulated, this notation will be used overall in this work.

Collision system	energy	centrality	N_{events}
Pb-Pb	$\sqrt{s_{NN}} = 2.76 \text{ TeV}$	0 – 10%	10^8
		40 – 60%	10^8

Table 5.1.1.: Number of produced π^0 for the studied centralities at LHC energies.

The produced pions p_T distribution is taken from [4], where the invariant yield was determined from a fit to data, and applied as a weight to the flat distributed pions. The number of produced π^0 as a function of p_T is shown in figure 5.1.1. Hence the centrality bin size is different for both classes, the more peripheral distribution has been normalized to the central one. The distribution is well described for centralities up to 60% by a powerlaw, with the parameters listed in table 5.1.2:

$$\frac{1}{2\pi p_T} \frac{d^2N}{dp_T dy} = a \cdot p_T^{-\left(b + \frac{c}{p_T^d + e}\right)} \quad (5.1.1)$$

The spatial distribution of the produced particles is flat in rapidity $|y| < 0.8$ and also in the whole azimuthal range of 2π since an anisotropic spatial distribution like elliptic flow would affect predominantly the statistics of the acceptance and is therefore, in the frame of this simple simulation, neglected.

centrality	a [1/GeV ²]	b	c	d	e
0 – 10%	25.53	5.84	-49.95	3.35	18.49
40 – 60%	4.18	5.67	-9.43	2.00	3.39

Table 5.1.2.: Paramaters for π^0 distribution for centralities studied in Pb-Pb collisions.

Although the spectra shown in figure 5.1.1 seem to be mostly parallel over the whole p_T range that is shown, an excess in the ratio of both yields can be seen in figure 5.1.2.

In between $p_T = 1$ GeV and $p_T = 4$ GeV, relatively more neutral pions are produced from the more central parameterization. This will influence the pion tagged photon acceptance in the given p_T region, since the distribution of the produced pions is a dominant factor that is put into the simulation.

5.2. Detector description

The pion decay tagged photon acceptance depends on the acceptance for the converted photon as well as the calorimeter acceptance for the unconverted photon. To estimate it and get a first impression of the systematic uncertainties that arise from the use of this method, a simple representation of the main features of the needed detectors is done. No full detector simulation is contained since a crucial feature is the geometric acceptance, which can easily be studied within this simple detector representation.

As described in section 4, TPC, EMCal and PHOS will be used for the PCM and calorimeter measurements respectively. Hereby are the detectors predominantly described through their geometric acceptance that is implemented in the simulation as well as a minimum energy a photon has to carry to induce a well-measurable shower in the electromagnetic calorimeters and a minimum transverse momentum on the TPC measurement that is needed for the produced electron-positron pair not to curl up inside the magnetic field. Although the simulation doesn't contain the conversion of the produced photons into electron-positron pairs inside the material of the TPC or the ITS, the minimum p_T is applied as the photon measured in the TPC is treated as a converted one.

The quantities describing the represented detectors are listed in table 5.2.1 and monitored for the produced photons. For the first estimation of the acceptance that is done in this work, the ITS is not essential and therefore not implemented in the representation of the detectors.

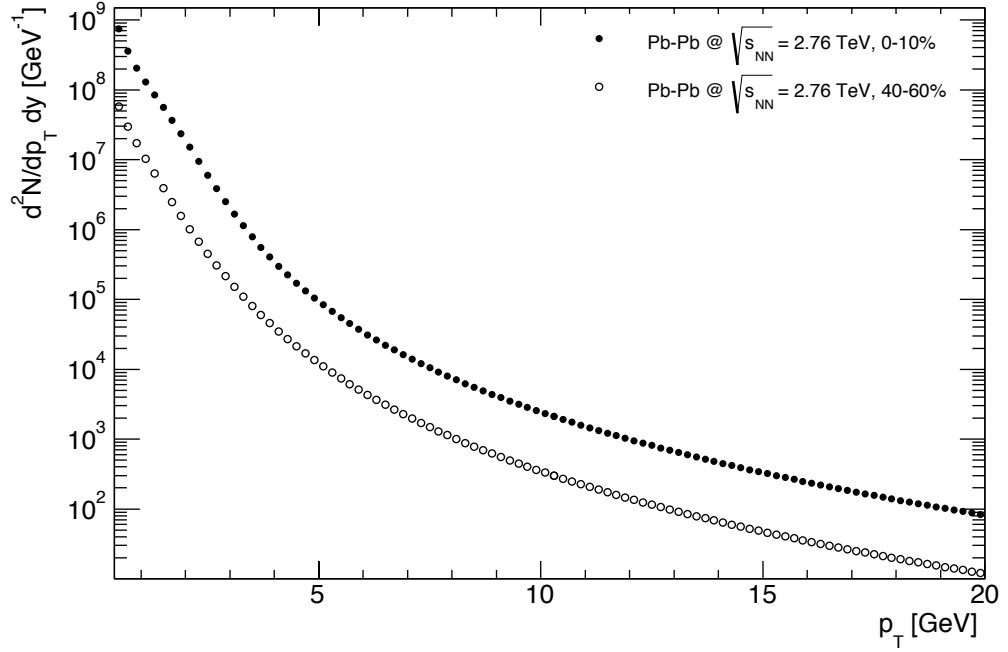


Figure 5.1.1.: p_T distribution of produced π^0 for Pb-Pb at $\sqrt{s_{NN}} = 2.76$ TeV.

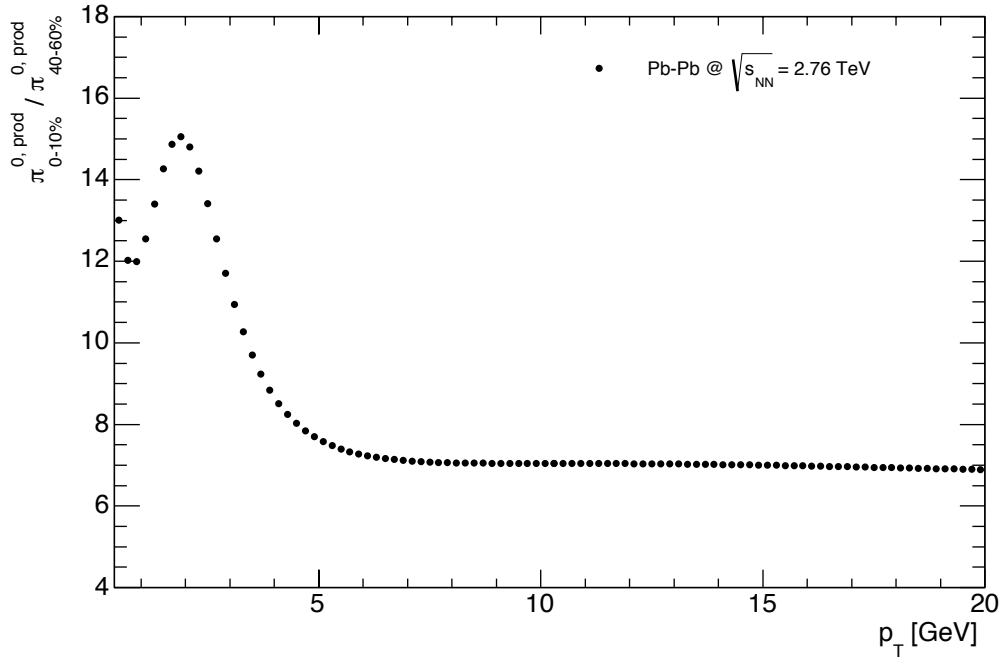


Figure 5.1.2.: Ratio of the produced pions p_T distributions for Pb-Pb at $\sqrt{s_{NN}} = 2.76$ TeV at 0 – 10% and 40 – 60% centrality, showing a relative excess for the more central parameterization in a given p_T range.

Detector	E_{min}	$p_{T,min}$	$ \eta $	ϕ
TPC	-	0.1 GeV	< 0.9	$[0; 2\pi]$
EMCal	0.5 GeV	-	< 0.7	$[80^\circ; 187^\circ]$
PHOS	0.3 GeV	-	< 0.12	$[260^\circ; 320^\circ]$

Table 5.2.1.: Detector representations used in the simulation.

5.3. Tagging acceptance

Pions that are produced as described in section 5.1 will decay with a branching ratio of more than 98% into two photons. It is then asked for the momentum, energy and spatial direction of the emitted photons. A photon is accepted as a converted photon, if it fulfills the requirements of the TPC representation from table 5.2.1. All photons accepted as converted ones give the measured converted photon spectrum $N_{\gamma_{conv}}(p_T)$. To each converted photon, the partner is searched for in the calorimeters. Since it is known, that every photon comes from the decay of a neutral pion, a converted photon with partner in a calorimeter will be tagged as coming from a π^0 decay. This gives the spectrum of converted photons tagged as coming from a π^0 decay: $N_{\gamma_{conv}}^{\pi^0 tag}(p_T)$. From these spectra we can calculate the pion tagged photon acceptance as a function of the converted photon p_T :

$$\langle \epsilon_\gamma(p_T) f(p_T) \rangle = \frac{N_{\gamma_{conv}}^{\pi^0 tag}(p_T)}{N_{\gamma_{conv}}(p_T)} \quad (5.3.1)$$

Since no full detector simulation is used, no statement about the efficiencies of the measurements can be made and $\epsilon_\gamma = 1$, for the whole p_T range. The calculation of $\langle \epsilon_\gamma(p_T) f(p_T) \rangle$ is done independently for both calorimeters and later combined. In figure 5.3.1 are the acceptances for both centrality classes pictured. Here the individual measurements for the single calorimeters have been combined. The relative errors that are shown are the systematic uncertainties that are implemented in the simulation. They will be discussed in detail in the following section. For both centralities, the acceptances

are comparable in value and uncertainty, although the shape for the most central class differs from the more peripheral one, starting at $p_T = 1$ GeV. Above $p_T = 4$ GeV the shapes of both acceptances start to coincide again. This feature can be explained from the relative excess in produced pions for the more central class, that was shown in figure 5.1.2. Since it is averaged over the transverse momentum of the produced pions, the pion decay tagged photon acceptance for 0 – 10% centrality falls below the acceptance for 40 – 60%. This effect fades to higher p_T , where the peak in the ratio of both produced π^0 spectra nearly vanished.

To study the systematic uncertainties of this method, the calculation of $\langle \epsilon_\gamma(p_T) f(p_T) \rangle$ has to be done separately for both calorimeters to pay attention to the different features of the calorimeters. Since both centrality classes produce nearly the same acceptances, this is done representatively for the most central class. Hereby it is assumed, that the dip in the acceptance that is observed doesn't affect the systematic uncertainties of the acceptance. The plot of the separated acceptances in figure 5.3.2 shows, that EMCal provides a greater acceptance due to the larger solid angle that is covered compared to PHOS. The systematic uncertainties for both calorimeters are nearly the same. Nevertheless it should be kept in mind that the acceptance for PHOS will carry a higher statistical uncertainty than for EMCal due to the smaller solid angle that is covered and therefore the smaller fraction of the acceptance that is contributed. Due to the scale of the plot it appears as if the suppression of the acceptance in between $p_T = 1$ GeV and $p_T = 4$ GeV arises from EMCal, but it is also present for PHOS, scaled to the acceptance. Also the combined acceptance is shown in the red solid points.

5.4. Systematics of tagging method

It was already seen, that the π^0 tagging method provides an acceptance that definitely exceeds zero and rises with p_T . To know if it is useful to apply this method, the systematic uncertainties have to be studied and compared to the default methods for the

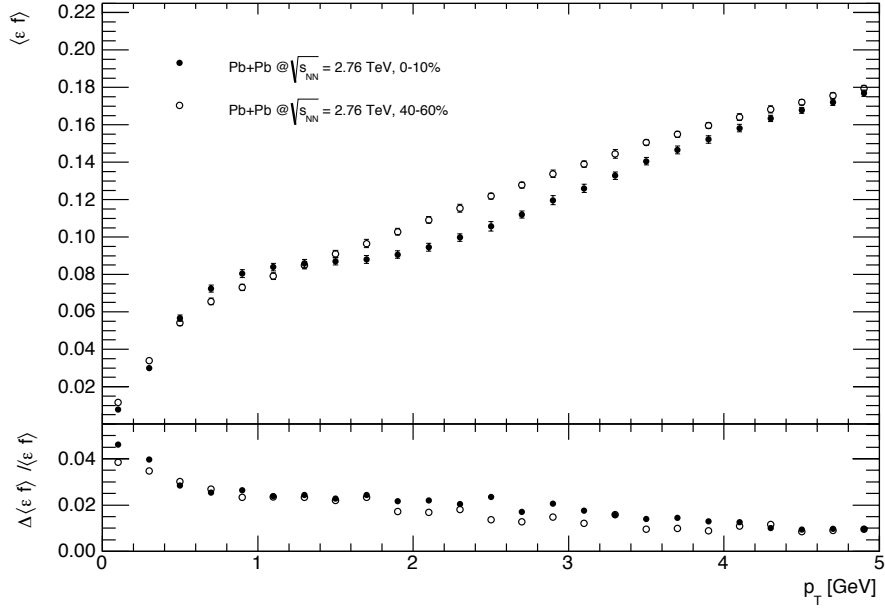


Figure 5.3.1.: π^0 tagged photon acceptance from simulation for the ALICE detector and the two centrality classes studied at LHC energies. The error bars and relative uncertainties in the lower plot are the quadratic sum of systematic uncertainties that are considered in the simulation.

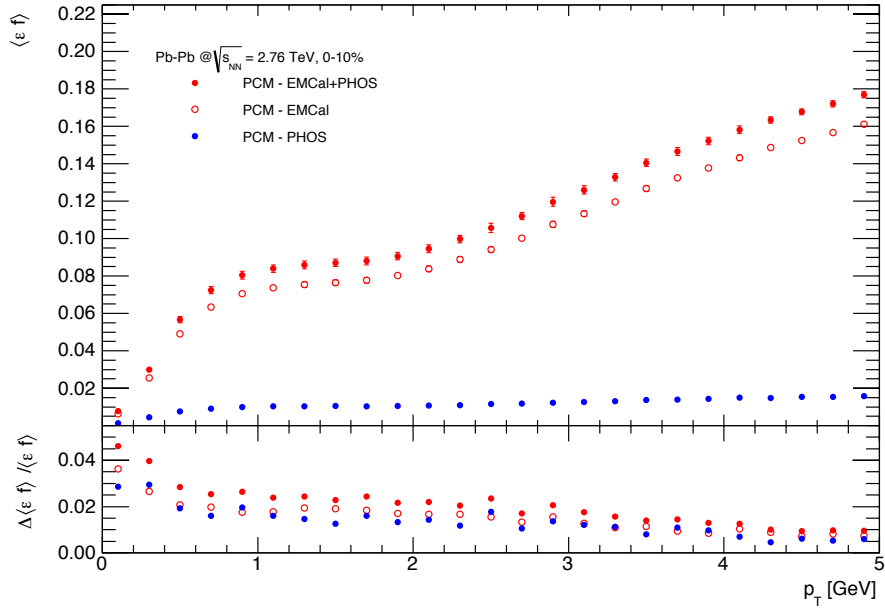


Figure 5.3.2.: π^0 tagged photon acceptance from simulation, separated for EMCal, PHOS and combined. The error bars and relative uncertainties in the lower plot are the quadratic sum of systematic uncertainties that are considered in the simulation.

calculation of the direct photon fraction used at ALICE. Although the conversion probability drops out in the formation of the double ratio, systematic uncertainties from the calorimeters will be carried by the efficiency and acceptance of the unconverted photon $\langle \epsilon_\gamma f \rangle$, that enters the double ratio as written in equation (3.3.3). These systematics will be discussed and summarized in this section to provide a standard for a comparison with PCM only and calorimeter only measurements. Some of the systematics are studied within the simulation, that are those from the energy scale and energy resolution of the calorimeters, whereas the remaining sources can't be studied in the frame of this simple simulation and are taken from previous analysis. The systematics that are implemented are put together for EMCAL in figure 5.4.1 and for PHOS in figure 5.4.2. A summary of all uncertainties, the acceptance is afflicted with, is presented in table A.2.1 and A.2.2 for EMCAL and PHOS respectively, that can be found in the appendix. The systematic uncertainties are studied for the most central class representatively.

The systematic uncertainties from the simulation for EMCAL (figure 5.4.1) and PHOS (figure 5.4.2) decrease with increasing p_T since they only affect the acceptance at the energy threshold of the calorimeters. If the energy of the unconverted photon is well above the minimum energy that is asked for, the effect of the uncertainty on the energy scale and resolution vanishes. Due to the lower statistics for the acceptance from PHOS, the corresponding uncertainties show more fluctuation than those from EMCAL.

Energy Scale A systematic uncertainty on the pion tagged photon acceptance will arise from the uncertainty within the calorimeter energy scale is known. In this simulation this comes from the discrepancy between the photon energy and the energy that the calorimeter cluster is assigned with. This plays a role at the position of the threshold that is needed for the detection of the unconverted photon. Therefore this systematic will affect the p_T distribution of the measured converted and tagged photons and propagate to the acceptance. The uncertainties on the energy scale for EMCAL [13] and PHOS [12] are listed in table 5.4.1, depending on the centrality class. Although a centrality-independent

uncertainty on the EMCal energy scale of 0.5% is given in [13], an uncertainty of 1.0% is used in this simulation to estimate the effect of different parameterizations of the non-linear behavior of the calorimeter on the energy scale at the position of the threshold. The uncertainty on the acceptance is estimated by varying the energy scale within the range it is known and comparing the results.

Calorimeter	Systematic uncertainty	
	0 – 10%	40 – 60%
EMCal	1.0	1.0
PHOS	1.0	0.5

Table 5.4.1.: Relative energy scale uncertainty.

Energy Resolution Although the parameters describing the energy resolution of the calorimeters are known, they may only be known within a certain range. This will propagate into the photon cluster energy and affect the tagged photon yield through variation of the photon energy especially at the threshold of the calorimeter. To study this effect a generous error on the parameters of 30% of the value is estimated. The acceptance is calculated with the correct parameters of the energy resolution as well as the ones, varied within their uncertainty and compared to estimate the systematic error arising. This will be a minor effect since it only plays a role at the energy threshold of the calorimeters and the energy is just smeared within a slightly wider range, wherefore the uncertainty of the energy resolution will be compensated partly.

Others EMCal There are also other sources of systematic uncertainties on the acceptance coming from EMCal, that can't be taken into account with this simulation and are taken from [13]. Since the systematics are given on the π^0 yield, at least some of them will not directly propagate to the pion tagged photon acceptance, but have to be adapted. These are the cluster cuts, the material budget and the acceptance of the different EMCal modules which will only affect one of the two photons coming from a π^0 decay and therefore only come into the acceptance with half the value. Neglected

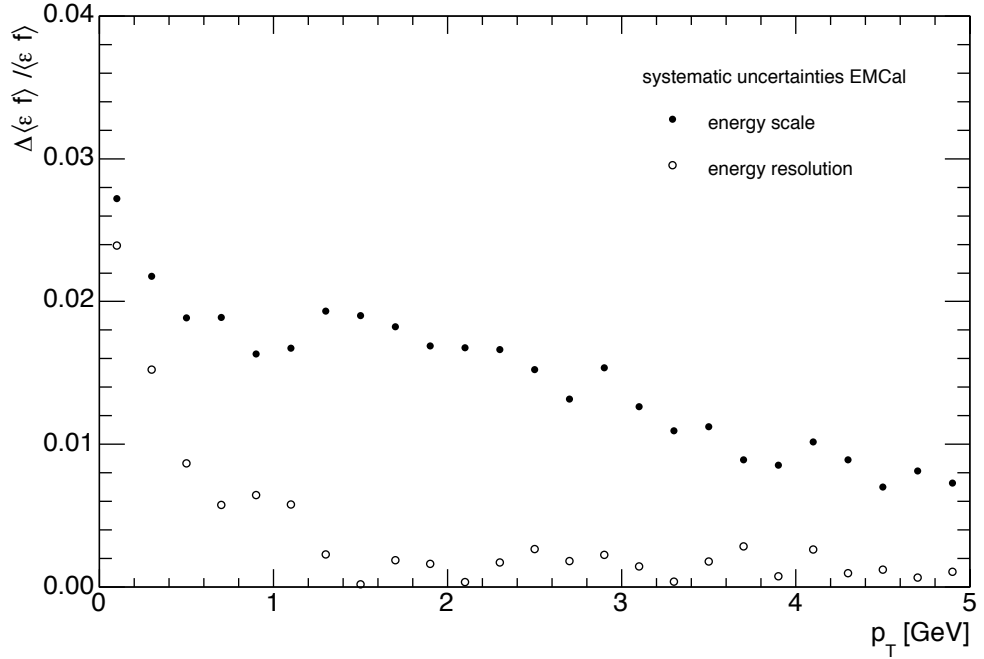


Figure 5.4.1.: Relative systematic uncertainties on pion tagged photon acceptance for EMCal from simulation for 0 – 10% centrality.

are the efficiency as well as the feed-down corrections since they don't play a role in the frame this simple simulation, where no imperfect behavior of the detectors or other electromagnetically decaying particles are considered. Every other source of systematic uncertainties mentioned in [13] propagates directly into the π^0 tagged photon acceptance.

Others PHOS For PHOS, the systematics that are not simulated are taken from [12], where the double ratio as well as it's uncertainties are calculated from a measurement of both photons from $\pi^0 \rightarrow \gamma\gamma$ in PHOS. Therefore all of the systematics mentioned that fit into the frame of this simulation affect the unconverted photon acceptance directly. Uncertainties that do not propagate into the acceptance are those referring to the hadron cocktail since only neutral pions are decayed in this simulation as well as the uncertainties from the feed-down correction and pileup of the π^0 yield.

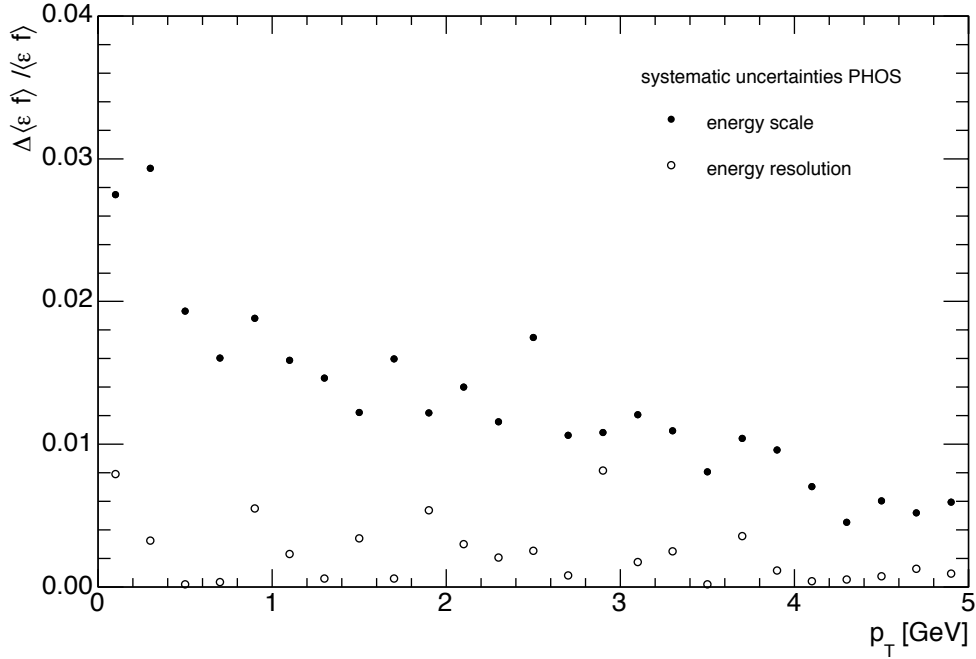


Figure 5.4.2.: Relative systematic uncertainties on pion tagged photon acceptance for PHOS from simulation for 0 – 10% centrality.

5.5. Validation of simulation procedure

The unconverted photon acceptance is also calculated from a simulation of the PHENIX detector at RHIC energies and compared to the results shown in section 3.3 to give a validation of the simulation procedure presented for the ALICE detector. If the acceptance calculated for PHENIX is comparable to the results from the full detector and event simulation presented in [7], the used procedure is assumed to be reasonable. Although it can't be expected to obtain the same values for the acceptance in this work, since some effects like imperfect efficiencies are left aside.

Decay simulation As for LHC energies the neutral pions are first produced flat in p_T with a parametrization of the distribution observed in the collision applied as a weight to gain more statistics to higher transverse momenta. The number of produced π^0 for the two centrality classes that will be simulated and studied at RHIC energies are shown in

table 5.5.1. Again two extreme centralities are chosen to see, if the pion tagged photon acceptance depends somehow on the centrality of the collision.

Collision system	energy	centrality	N_{events}
Au-Au	$\sqrt{s_{NN}} = 200 \text{ GeV}$	0 – 10%	10^8
		80 – 92%	10^8

Table 5.5.1.: Number of produced π^0 for the studied centralities at RHIC energies.

The neutral pion p_T shape is parameterized from a fit to data in [7] with the invariant Hagedorn function shown in equation (5.5.1). The parameters describing the p_T distribution for the two centrality classes are listed in table 5.5.2.

$$\frac{1}{2\pi p_T} \frac{d^2N}{dp_T dy} = A \left(e^{-(ap_T + bp_T^2)} + \frac{p_T}{p_0} \right)^{-n} \quad (5.5.1)$$

centrality	A [1/GeV ²]	a [1/GeV]	b [1/GeV ²]	p_0 [GeV]	n
0 – 10%	1331.0	0.5654	0.1945	0.7429	8.361
80 – 92%	51.1	0.2470	0.0619	0.7101	8.453

Table 5.5.2.: Parameters for π^0 distribution following equation (5.5.1) for studied centralities in Au-Au collisions.

Compared to the p_T shape for Pb-Pb collisions at LHC energies, the spectra falls more steeply as it can be seen in figure 5.5.1, where the simulated π^0 distribution is shown. Comparatively less neutral pions are produced at higher transverse momenta. The produced pions are decayed and the photons from $\pi^0 \rightarrow \gamma\gamma$ are searched for in the representation of the PHENIX detector.

Detector description The PHENIX detectors, shown in figure 5.5.2, that will be used for the determination of the pion tagged photon acceptance in this work are the Drift Chambers (DC) to measure the tracks of charged particles as well as the electromagnetic calorimeters: PbGl and PbSc which are lead glass Cherenkov detectors and lead

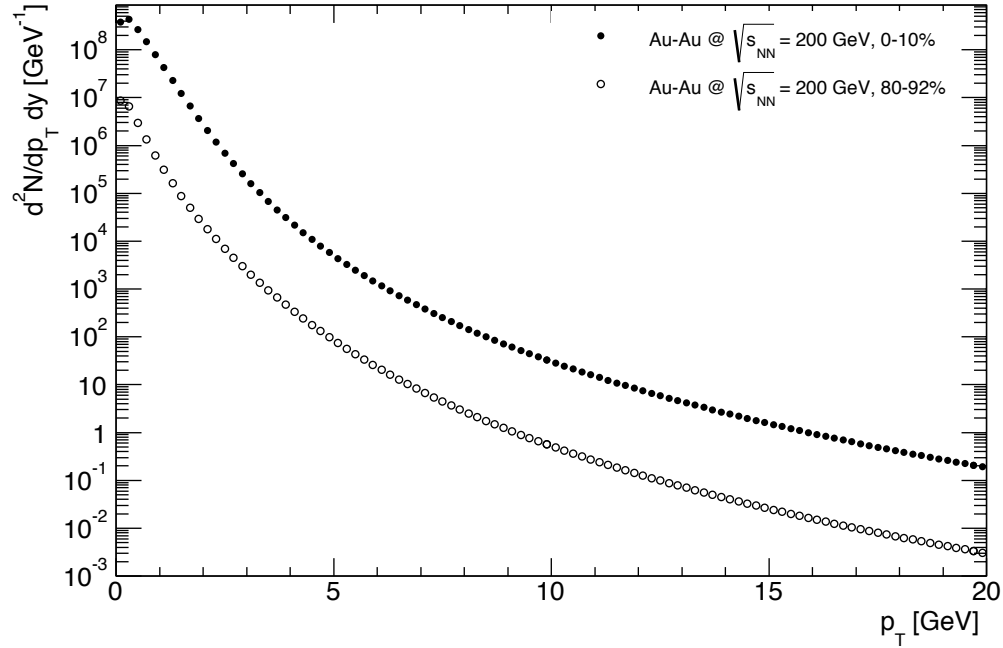


Figure 5.5.1.: p_T distribution of produced π^0 for Au-Au at $\sqrt{s_{NN}} = 200$ GeV.

scintillators respectively. The energy resolution for the calorimeters can be described by equation (4.3.1) with the parameters $a = 8.1 \pm 2.4\%$ and $c = 2.1 \pm 0.6\%$ for PbSc and $a = 6.0 \pm 1.8\%$ for PbGl. Parameters not mentioned equal zero in this description of the energy resolution.

In contrast to the ALICE experiment, no detector covers the full range in azimuth as the detectors are separated in two arms. The DC and the combined calorimeters cover nearly the same solid angle, which leads to a higher conditional probability for the unconverted photon to hit a calorimeter if the partner was measured in a drift chamber, since the opening angle of the photon pair will be small due to the highly relativistic energies and further decrease with increasing p_T .

Again no full detector simulation is applied, instead the needed parts will be represented by the quantities [7] listed in table 5.5.3. These are again the geometric acceptance as well as a minimum energy for the calorimeters and a minimum p_T for DC.

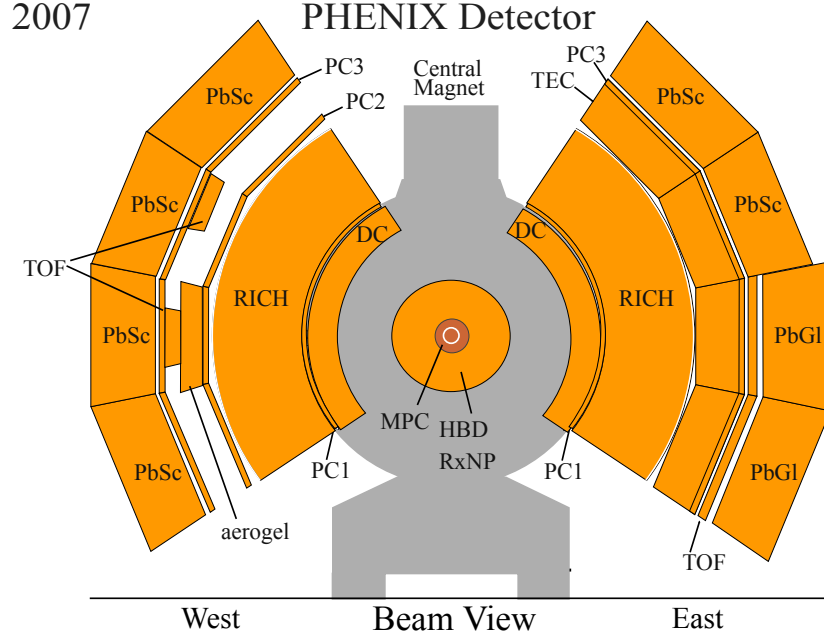


Figure 5.5.2.: Cut in transverse plane through the PHENIX detector, showing the DC, PbSc and PbGl in the two detector arms. [7]

Detector	E_{min}	$p_{T,min}$	$ \eta $	ϕ
DC	-	0.4 GeV	< 0.35	$[-33.75^\circ; 56.25^\circ]$ $[123.75^\circ; 213.75^\circ]$
PbSc	0.6 GeV	-	< 0.375	$[11.25^\circ; 56.25^\circ]$ $[123.75^\circ; 213.75^\circ]$
PbGl	0.6 GeV	-	< 0.375	$[-33.75^\circ; 11.25^\circ]$

Table 5.5.3.: PHENIX detector representations used in the simulation.

Calculation of pion tagged photon acceptance As described in section 5.3, the spectrum of converted photons with partners in calorimeters is measured and divided by the spectrum of all converted photons, giving $\langle \epsilon_\gamma(p_T) f(p_T) \rangle$ as a function of the converted photon p_T , with the efficiency set to one. This is done for both calorimeters independently and then combined since the interest lies in a comparison with the acceptance from [7], shown in figure 3.3.1. The calculated acceptance is shown for both centrality classes in figure 5.5.3. The error bars in the plot are the quadratic sum of the two simulated sources of systematic uncertainties. It is estimated, that the energy scale is only

known within a deviation of 2% [7] which results in a deviation of the acceptance. Also a generous uncertainty of 30% on the parameters of the calorimeters energy resolution is assumed, that propagates into the acceptance.

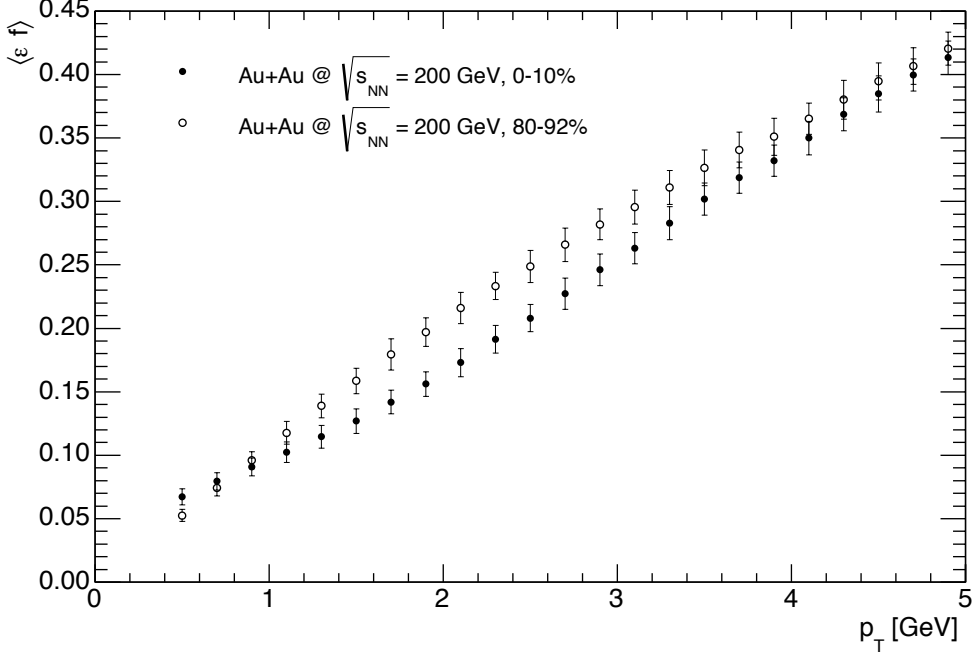


Figure 5.5.3.: π^0 tagged photon acceptance from simulation for the PHENIX detector at RHIC energies. The error bars are a quadratic sum of systematic uncertainties arising from an uncertainty on the calorimeters energy scale and energy resolution.

As expected, the acceptance in figure 5.5.3 does not change much in shape and value for the two centrality classes shown which is due to the correspondence of the two parameterizations for the produced pions used. Again a slight suppression for the more central class can be observed, as it is present for the acceptance determined with the ALICE detector at LHC energies. Also the acceptance for both centralities is comparable in shape to the one pictured in figure 3.3.1. The acceptance in this simulation rises slightly stronger since no additional suppressing effects like imperfect efficiencies are considered as they are in [7], where a full detector and event simulation is used. Still the comparison of these two plots assures that the simulation shows a reasonable behavior of the pion tagged photon acceptance and should therefore allow an estimation of the

applicability of this method for the ALICE detector from the simulation procedure presented in this work.

6. Conclusion

The simulation presented in the previous section already showed, that the pion tagged photon acceptance determined with the ALICE detector at LHC energies takes values up to roughly 16 – 18%. As expected this is mostly independent from the centrality of the collision. Although a perfect efficiency is assumed in the frame of this simple simulation, the acceptance should not drop remarkably when considering a behavior closer to reality, as it can be seen from the comparison of the acceptances of the PHENIX detector simulated in this work and the results from [7]. But to see if the tagging method brings any advantage to the default methods used in ALICE, the systematic uncertainties of the photon double ratio that result from the different methods have to be compared. The total relative systematic uncertainties for central collisions are listed representatively for several p_T bins in table 6.0.1.

Method	Total relative systematic uncertainty		
	$p_T = 1$ GeV	$p_T = 2$ GeV	$p_T = 3$ GeV
PCM - PCM	10.5	6.5	8.0
PHOS - PHOS		7.5	
PCM - PHOS		7.2	
PCM - EMCal	5.3 – 13.6		5.0 – 6.1

Table 6.0.1.: Total relative systematic uncertainties on the photon double ratio for the different methods for π^0 reconstruction. The method notation implies how the two photons were measured.

It should be noted, that the systematics for the tagging method are rather underestimated since in the course of this work the pion tagged photon acceptance is assumed

to be the single source of systematic uncertainties left in the double ratio formed from equation (3.3.3), which must not be true in general. Also the systematic uncertainties taken from previous analysis are transferred to fit into the frame of the simulation and some of those are left aside.

Nevertheless are the uncertainties arising from the tagging method of the same order as those from the conversion method or from calorimeter measurements. Due to the very good resolution of the conversion method to low transverse momenta as well as the very good known material budget, the combination of conversion and calorimeter measurements should not be able to produce better results to low p_T . With increasing transverse momentum, the calorimeter measurements should start to gain resolution in comparison to the conversion measurements. At intermediate p_T , the tagging method, at least as it was studied in this works, produces lower systematic uncertainties than conversion only as it can be seen in table 6.0.1 for $p_T = 3$ GeV. Since the systematic uncertainties of the tagging method are comparable to those of the default methods, the pairing of conversion and calorimeter photons should be beneficial for cross-checks to the default methods. Also the tagging method may be useful in an intermediate p_T region due to the expected behavior of its resolution.

7. Outlook

It has already been shown, that the tagging method will in principle be applicable with the ALICE detector and the estimation of the systematic uncertainties of this method suggests, that it may be used for cross-checks with the default methods. To get an idea how the different methods behave, some π^0 analysis for p-Pb collisions at $\sqrt{s_{NN}} = 5.023$ TeV with data taken with the ALICE detector have been done. The neutral pions were reconstructed from the two photon decay channel, using photon-pairs from:

- PCM - PCM
- PCM - PHOS
- PCM - EMCal

In figure 7.0.1 the different invariant masses of the reconstructed neutral pions are shown over p_T . It can be seen, that all methods are able reproduce the real π^0 mass of $m_{\pi^0} \approx 0.135$ GeV within a reasonable range, although PCM - PHOS and PCM - EMCal show a different behavior below $p_T = 1$ GeV, which is due to the fitting in this range, where nearly no signal exceeds the background. Since the calorimeters have some minimum energy that is needed for an well-measurable electromagnetic shower to emerge and the energy resolution increases with the energy of the incident particle, it is not surprising to observe a deviation from the real π^0 mass to very low p_T for the reconstruction from the combination of photons from conversion and calorimeter measurements.

The differences in resolution of the different methods can be seen in figure 7.0.2, where the widths of the fitted peaks are shown. Again the combination methods show no representative values to very low p_T , which is due to the difficult fitting in this region. Since the photon conversion method offers a very good resolution to lower p_T , a slight rise of the peak widths with transverse momentum can be observed for this method. Nevertheless shows the conversion method an advantage to the combination methods over the whole p_T range that is shown. For both combination methods, the resolution increases with transverse momentum which is due to the behavior of the energy resolution of the calorimeters. Therefore the combination of conversion and calorimeter photons should give a better resolution to higher p_T than taking conversion photons only. PHOS offers a slightly better resolution for the combination method than EMCal in the lower p_T range, since it has better energy resolution to lower energies. This confirms the expectation, that the combination of conversion and calorimeter photons could be a good way to measure at transverse momenta where the conversion method starts to lose resolution or to do cross-checks with the default methods for π^0 reconstruction used at ALICE.

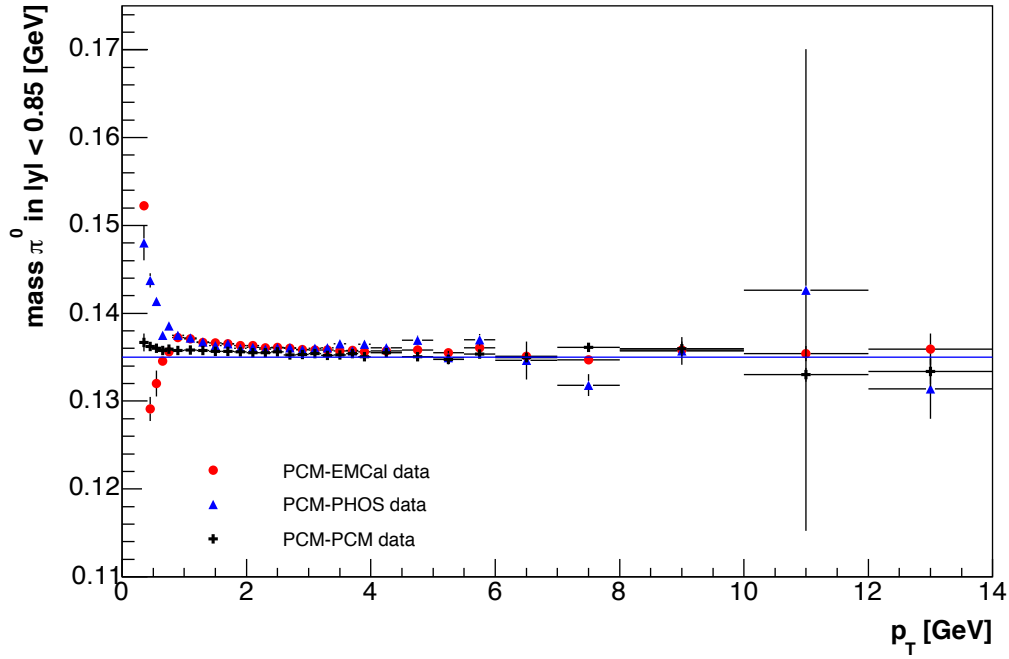


Figure 7.0.1.: Reconstructed π^0 peak position over p_T for different methods with m_{π^0} represented by the blue line.

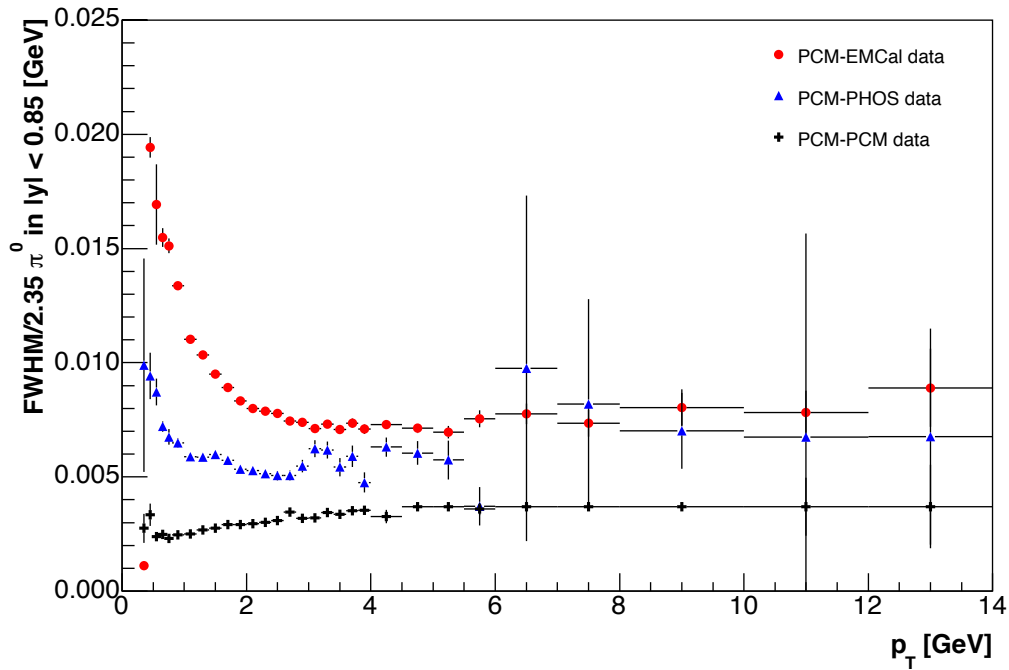


Figure 7.0.2.: Reconstructed π^0 peak widths for the different methods, referring to the different resolutions.

8. Bibliography

- [1] P. Braun-Munzinger and J. Stachel. *The quest for the quark gluon plasma*. Nature, 448(7151):302-309, 2007.
- [2] ALICE Collaboration, *Performance of the ALICE Experiment at the CERN LHC*, CERN-PH-EP-2014-031, 2014.
- [3] ALICE Collaboration, *ALICE Electromagnetic Calorimeter Technical Design Report*, CERN-LHCC-2008-014, 2008.
- [4] ALICE Collaboration, *Neutral pion production at midrapidity in pp and Pb-Pb collisions at $\sqrt{s_{NN}} = 2.76$ TeV*, CERN-PH-EP-2014-091, 2014.
- [5] H. Torii (for the ALICE-PHOS Collaborations), *The ALICE PHOS Calorimeter*, J. Phys. Conf. Ser. 160 012045, 2009
- [6] F. Bock, *ALICE Capabilities for Studying Photon Physics with the Conversion Method at LHC Energies*, Bachelor Thesis at the Physikalisches Institut at the University of Heidelberg, 2010
- [7] R. M. Petti, *Low Momentum Direct Photons as a Probe of Heavy Ion Collisions*, Dissertation at the Stony Brook University, 2013
- [8] ALICE Collaboration, K Aamodt et al, *The ALICE experiment at the CERN LHC*, JINST 3, S08002, 2008

- [9] R. J. Fries and B. Müller, *Heavy Ions at LHC: Theoretical Issues*, The European Physical Journal C-Particles and Fields, 34:279-285, 2004
- [10] P. Stankus, *Direct photon production in relativistic heavy-ion collisions*, Annu. Rev. Nucl. Part. Sci. 2005. 55:517-54, 2005
- [11] M. Wilde, F. Bock, D. Lohner, A. Marìn, K. Reygers, C. Klein-Bösing, A. Passfeld for ALICE Collaboration, *Analysis Note: Measurement of Direct Photons in pp Collisions at the LHC with ALICE at $\sqrt{s} = 7$ TeV and Pb-Pb Collisions at $\sqrt{s_{NN}} = 2.76$ TeV via Conversions*, ALICE-ANA-2012-xxx, 2014
- [12] D. Peressounko, D. Blau, Y. Kharlov, B. Polishchuk, *Direct photon production in Pb-Pb collisions at $\sqrt{s_{NN}} = 2.76$ TeV measured with ALICE PHOS*, ALICE-INT-2012-xxx, 2014
- [13] Jason Kamin, Haitao Zhang, Baldo Sahlmüller, *π^0 Measured by the EMCal in pp collisions at $\sqrt{s} = 2.76$ TeV*, ALICE-ANA-2013-1024, 2014
- [14] ALICE Collaboration, *Photoproduction of ρ^0 in ultra-peripheral nuclear collisions at ALICE*, J. Phys. Conf. Ser. 455 (2013) 012010, 2013

A. Appendix

A.1. Systematic uncertainties on photon double ratio

Centrality p_T	0 – 20%		20 – 40%		40 – 80%	
	2 GeV	10 GeV	2 GeV	10 GeV	2 GeV	10 GeV
Inclusive photons						
Efficiency	3.0	3.0	0.7	0.7	2.5	2.5
Contamination	2.0	2.0	1.3	1.3	2.9	0.5
Conversion	1.7	1.7	1.7	1.7	1.7	1.7
Acceptance	1.0	1.0	1.0	1.0	1.0	1.0
π^0 yield						
Raw Yield extraction	2.7	4.0	3.1	5.2	1.8	2.9
PID cuts	1.2	1.2	1.7	1.7	1.7	1.7
Efficiency	1.4	1.3	2.1	1.4	1.9	1.1
Acceptance	1.0	1.0	1.0	1.0	1.0	1.0
Per module yield	4.0	4.0	4.0	4.0	4.0	4.0
Pileup	1.0	1.0	1.0	1.0	1.0	1.0
Feed-down correction	2.0	2.0	2.0	2.0	2.0	2.0
Cocktail						
Shape of π^0 spectrum	1.3	4.3	1.8	1.8	1.8	1.8
η/π^0 ratio	2.2	1.7	2.2	1.6	2.1	1.6
K_s^0/π^0 ratio	0.3	0.3	0.4	0.3	0.4	0.4
ω/π^0 ratio	0.6	0.6	0.5	0.5	0.5	0.5
Double ratio total	7.5	8.9	7.3	8.1	7.6	7.1

Table A.1.1.: Relative systematic uncertainties on photon double ratio, measured with PHOS at ALICE for Pb-Pb collisions at $\sqrt{s_{NN}} = 2.76$ TeV for different centrality classes. [12]

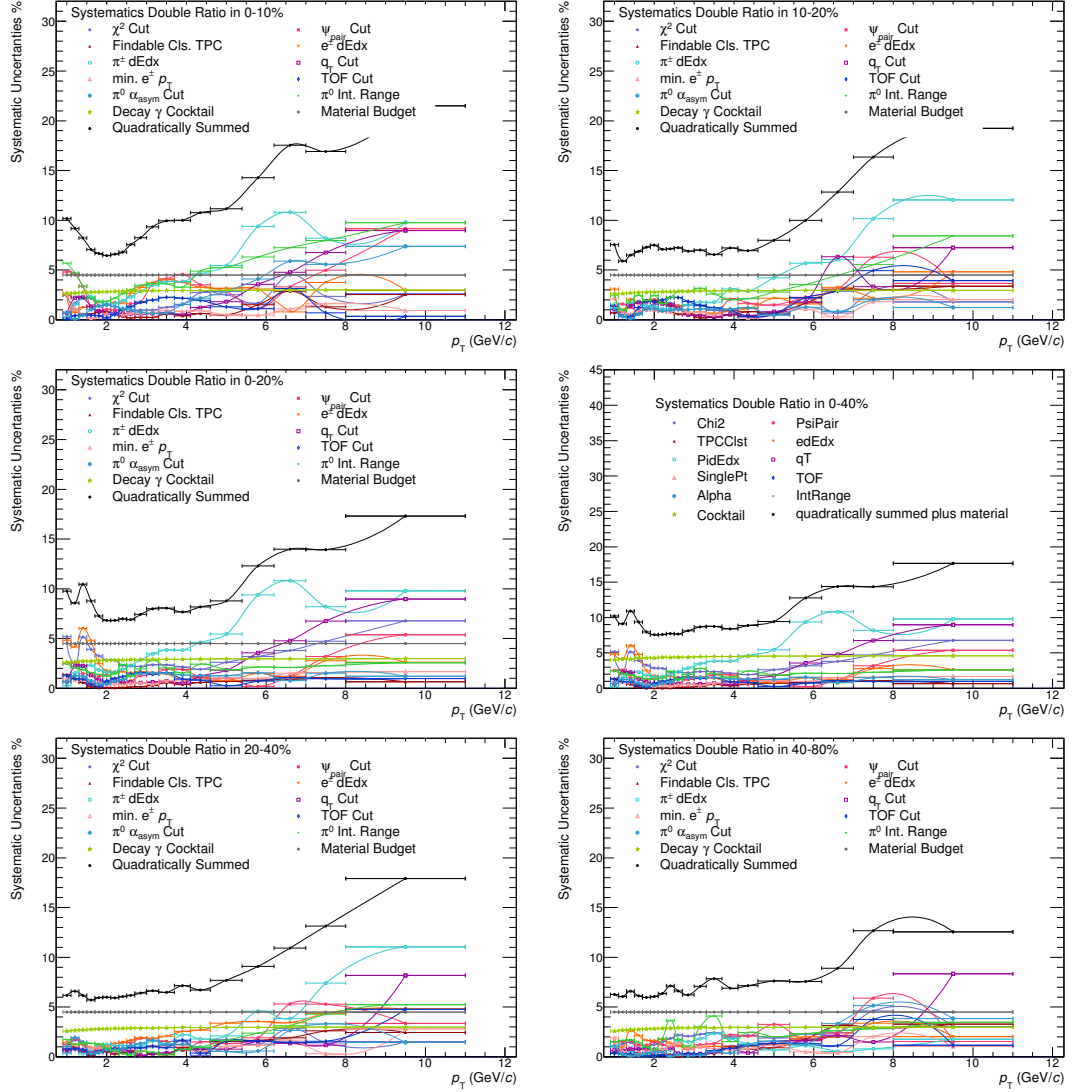


Figure A.1.1.: Systematic uncertainties on photon double ratio, measured with PCM at ALICE for Pb-Pb collisions at $\sqrt{s_{NN}} = 2.76$ TeV for different centrality classes. [11]

A.2. Systematic uncertainties on pion tagged photon acceptance

Systematic uncertainty component	Relative uncertainty	
	$p_T = 1 \text{ GeV}$	$p_T = 3 \text{ GeV}$
energy scale	1.6%	1.2%
energy resolution	< 1%	< 1%
clusterizer	2 – 10%	2 – 4%
cluster cuts, bkg subtraction	3%	3%
yield extraction	2 – 8%	1.5%
material budget	1%	< 1%
acceptance	2.5%	2.5%
total uncertainty	5.3 – 13.6%	5.0 – 6.1%

Table A.2.1.: Systematic uncertainties on pion tagged photon acceptance for EMCal.

Systematic uncertainty component	Relative uncertainty
	$p_T = 2 \text{ GeV}$
energy scale	1.4%
energy resolution	< 1%
Inclusive photons	
efficiency	3.0%
acceptance	1.0%
contamination	2.0%
conversion	1.7%
non-linearity	2.2%
π^0 yield	
raw yield extraction	2.7%
PID cuts	1.2%
efficiency	1.4%
acceptance	1.0%
per module yield	4.0%
total uncertainty	7.2%

Table A.2.2.: Systematic uncertainties on pion tagged photon acceptance for PHOS.

Erklärung

Ich versichere hiermit, dass ich diese Arbeit selbständig verfasst habe und keine anderen als die angegebenen Quellen und Hilfsmittel benutzt habe.

Heidelberg, den 8. September 2014